

# Gravitational Lensing Constraints on Dynamical and Coupled Dark Energy

G La Vacca<sup>1,3</sup> and L P L Colombo<sup>2,3,4</sup>

<sup>1</sup> Dipartimento di Fisica Teorica e Nucleare, Università di Pavia, via A. Bassi, 6 I-27100 Pavia, Italy

<sup>2</sup> Dipartimento di Fisica “G Occhialini”, Università di Milano-Bicocca, Piazza della Scienza, 3 I-20126 Milano, Italy

<sup>3</sup> INFN Sezione di Milano-Bicocca

<sup>4</sup> Department of Physics & Astronomy, University of Southern California, Los Angeles, CA 90089-0484

E-mail: Giuseppe.Lavacca@mib.infn.it

**Abstract.** Upcoming Weak Lensing (WL) surveys can be used to constrain Dark Energy (DE) properties, namely if tomographic techniques are used to improve their sensitivity. In this work, we use a Fisher matrix technique to compare the power of CMB anisotropy and polarization data with tomographic WL data, in constraining DE parameters. Adding WL data to available CMB data improves the detection of all cosmological parameters, but the impact is really strong when DE–DM coupling is considered, as WL tomography can then succeed to reduce the errors on some parameters by factors  $> 10$ .

## 1. Introduction

The first data system requiring Dark Energy (DE) concerned cosmic acceleration, detected through high-redshift supernovae [1]. CMB [2] and deep sample [3] data supported also the DE case, showing that the density parameter for non-relativistic matter  $\Omega_{0,m} \sim 0.3$ , while the total density parameter  $\Omega_0 \sim 1$ .

In the most popular scenario, DE is ascribed to a cosmological constant  $\Lambda$ . Alternative options include a self-interacting scalar field,  $\phi$  (quintessence or dynamical DE [4, 5]) and modifications of General Relativity [6].

It is known that models with  $\Lambda$  ( $\Lambda$ CDM) apparently accommodate all available data systems. The problem is the physical origin of  $\Lambda$ , which can be a false vacuum; this however causes well known *fine tuning* and *coincidence* problems.

The former problem is partially eased in dynamical DE (dDE) scenarios, when self interaction is due to a *tracking* potential  $V(\phi)$  [7]. If  $V(\phi)$  is SUGRA [5], the fit with data is at least as good as for  $\Lambda$ CDM [8].

In the attempt to ease the coincidence problem, DM–DE interaction (e.g., [9, 10]) was also considered, yielding an energy transfer between the dark components, so

allowing a (quasi)–parallel scaling of DM and DE from a fairly high redshift until the present. While laboratory data set no significant constraint on DM–DE interaction strength, parametrized by  $\beta$  (see below), recent works placed constraints on possible couplings, by using SNIa data [11] or the redshift evolution of the Hubble parameter,  $H$  [12]. Accordingly,  $\beta > 0.12$ – $0.15$  [13, 14] is hardly consistent with observations.

Unfortunately, such a low coupling level no longer eases the coincidence problem [15], but, once the genie has come out from the lamp, it is hard to put it back inside. The point is whether low values of  $\beta$ , as allowed by current data, can interfere with future data analysis. In particular, when we allow for non–zero  $\beta$ , how do errors on other parameters behave?

In this work we tried to answer this question by using a Fisher matrix technique. We considered two different models, set by similar values of cosmological parameters, without and with coupling. In the latter case, we took  $\beta = 0.1$ . Starting from these models, we evaluated the expected errors on cosmological parameters, as obtained when data concern just CMB anisotropy and polarization or include tomographic weak lensing (WL).

As a matter of fact, in coupled models, the time evolution of the dark components is non–standard. If such models are considered in a Newtonian approximation, it is as though DM particles had a  $\phi$ –dependent mass. Also for quite low  $\beta$ 's, this anomalous scaling leaves an imprint on both the expansion history of the Universe, and the growth of (matter) fluctuations, at the linear and non–linear levels (e.g. [16]).

However, any detected evolution of  $H$  can be reproduced through a suitable redshift dependence of DE density  $\rho_{de}$  and state parameter  $w_\phi$ , when  $\phi$  approaches  $m_p$  (the Planck mass). A risk is that, if matter and dark energy are coupled, fitting observations leads to an estimate of a phantom equation of state ( $w_\phi < -1$ ), even if  $w_\phi > -1$  at all redshifts [17].

In principle, this risk can be excluded if the redshift dependence of the growth factor  $G(z)$  is also tested, through the increase in number and concentration of bound systems. Data providing information both on  $H(z)$  and  $G(z)$  are therefore able to discriminate between coupled and uncoupled models. Experiments, or combinations of experiments, probing  $H(z)$  and  $G(z)$  are then needed.

CMB data, used to constrain coupling [13, 18], place only upper limits on  $\beta$ . The analysis of Ly– $\alpha$  and the matter power spectrum of the 2dF and SDSS surveys [14] does not lead to great improvements. At the available sensitivity level, such data systems provide just weighted integrals of  $H(z)$  and  $G(z)$ , which remain consistent with a rather wide set of options.

On the contrary, gravitational lensing, alone or in combination with CMB data, was already shown to be a powerful tool for the analysis of DE. WL tomography probes the power spectrum  $P(k)$  at different redshifts and is thus well suited to constrain  $G(z)$ .

In this work we aim to put these conceptual points on a more quantitative basis and to deepen the case of coupling, by performing a Fisher analysis of future WL surveys and CMB experiments.

The outline of this work is as follow. In Sec. 2 we review the basic properties and definitions of dDE models and WL, in Sec. 3 we show the results of the Fisher analysis, in Sec. 4 we discuss them and in Sec. 5 we summarize our findings and draw our conclusions.

## 2. Models and definitions

### 2.1. Interacting Dark Energy

We consider a cosmological model where the DE field  $\phi$  interacts with the cold DM component. The model requires the specification of the potential  $V(\phi)$  and the function  $f(\phi)$  characterizing the coupling. The equation of motion for  $\phi$  then reads

$$\ddot{\phi} + 3H\dot{\phi} = -V_{,\phi}^{eff} \quad \text{with} \quad V^{eff} = V + \rho_c . \quad (1)$$

Here dots denote ordinary time differentiation,  $H(a) = \dot{a}/a$  and  $\rho_c$  is DM energy density. In turn, its evolution is governed by

$$\dot{\rho}_c + (3H + C\dot{\phi})\rho_c = 0 , \quad \text{with} \quad C(\phi) = \frac{d \log(f)}{d\phi} . \quad (2)$$

This equation can be integrated and gives:

$$\rho_c(a) = \rho_{c,0} a^{-3} f(\phi) . \quad (3)$$

For  $f = 1$  eqs. (1), (3) return ordinary dDE equations. The equations for the other components remain unchanged. In a generic coupled model, then, the ratio between the energy densities of cold DM and baryons is not fixed, but evolves in time according to  $f(\phi)$ .

However, it is always possible to define an effective DE component of density

$$\rho_{de}^{eff}(a) = \rho_c a^{-3} [f(\phi) - 1] + \rho_{de}(a) . \quad (4)$$

In general,  $\rho_{de}^{eff}(a)$  is not guaranteed to be positive and detecting  $\rho_{de}^{eff}(a) < 0$  would be a clear indication that our description of the dark sector is not adequate. Lacking such clear giveaway, however, experiments probing  $H(z)$  can hardly discriminate between DE-DM interaction and an *ad hoc* DE component. If its effective state parameter  $w^{eff} (= p^{eff}/\rho^{eff})$  is  $< -1$ , data may appear to require phantom DE (see [19] for discussion).

Coupling affects also fluctuation growth. In the Newtonian limit, *i.e.* well below the horizon, and neglecting the contribution of radiation, baryons and DM fluctuations grow according to the equations (e.g. [16, 20]):

$$\begin{aligned} \ddot{\delta}_b + 2H\dot{\delta}_b &= 4\pi G(\rho_b\delta_b + \rho_c\delta_c) \\ \ddot{\delta}_c + 2H\dot{\delta}_c &= 4\pi G[\rho_b\delta_b + (1 + \frac{4}{3}\beta^2)\rho_c\delta_c] , \end{aligned} \quad (5)$$

where we defined  $\beta$  so that

$$C(\phi) = 4\sqrt{\frac{\pi}{3}} \frac{\beta(\phi)}{m_p} , \quad (6)$$

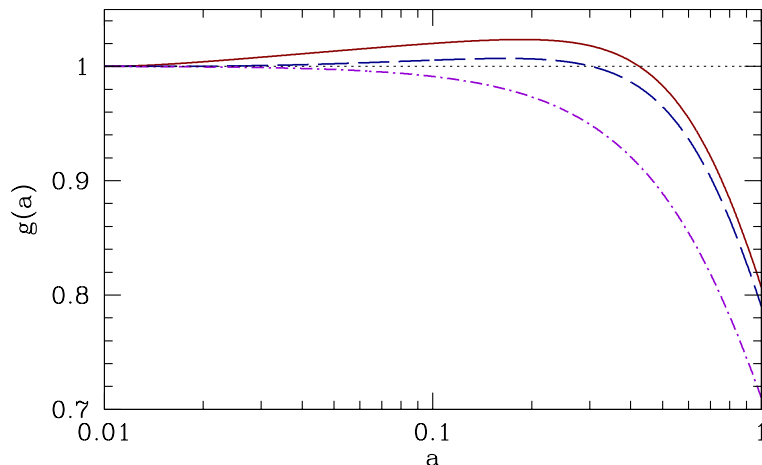


**Figure 1.** The growth suppression rate  $g(a) \equiv \delta(a)/a$  for CDM (solid line) and baryons (dashed line) in a coupled model. Curves refer to a SUGRA potential with exponential coupling. It can be noticed that the cold dark matter evolution rapidly diverges from the standard cold dark matter solution,  $g(a) = 1$  (dotted line), even well into the matter dominated era. For comparison, we also plot  $g(a)$  for the same SUGRA model with coupling turned off (dot-dashed line).

while  $m_p = G^{-1/2}$ . Therefore, baryons and DM perturbations grow at different rates and, even soon after recombination, a growing mode  $\delta \propto a$  no longer exists (see Fig. 1), leading to a bias between baryon and DM perturbations. Analytical models of spherical collapse have shown that this differential growth results in a baryon–DM segregation, with baryons occupying the outer regions of collapsed objects [21].

Eqs (5) also show that the growth equations explicitly depend on both  $H$  and  $\rho_c$ ; therefore, if we measure the growth from data, a possible anomalous scaling can no longer be masked though an *ad-hoc* definition of an effective DE density. It is then licit to conclude that experiments probing the rate of growth of fluctuations are in principle well suited to test coupling between the dark components.

In this work we are interested to combining WL and CMB data, which cannot be accurately described using current parametrisations [22]. Therefore, we follow a more conventional approach and choose the functional forms

$$V(\phi) = \frac{\Lambda^{4+\alpha}}{\phi^\alpha} \exp\left(4\pi \frac{\phi^2}{m_{\text{PL}}^2}\right), \quad f(\phi) = \exp\left(\beta \sqrt{\frac{8\pi}{3}} \frac{\phi_0 - \phi}{m_{\text{PL}}}\right) \quad (7)$$

The SUGRA [5] potential  $V(\phi)$  depends on the slope  $\alpha$  and the energy scale  $\Lambda$ . Fixing DE density today and  $\Lambda$  ( $\alpha$ ), however, determines a unique value of  $\alpha$  ( $\Lambda$ ). CMB, SNIa and deep sample data yield  $\Lambda \lesssim 10^3 \text{GeV}$  [8], in the absence of coupling. Here we focus on the SUGRA potential as it naturally arises in the context of Supergravity Theories and is an example of tracking potential characterized by a rapid time variation of the equation of state, when DE becomes dominant. Therefore, assuming a constant  $w$  for this class of potential may lead to misleading results. Different choices for the potential are clearly possible.

The coupling function  $f(\phi)$  depends on  $\beta$ , and  $\phi_0$  is the field value today. In this work we assume a constant  $\beta \geq 0$  (see however [19] for a different approach); data place the upper limit  $\beta \lesssim 0.12 - 0.15$  [13, 14]. For reasonable values of the cosmological parameters and of  $\Lambda$ , we expect coupling effects not to be relevant for  $\beta \lesssim 0.01$ , so that the dynamically interesting values for the coupling lies in the range  $0.01 < \beta < 0.10$ .

## 2.2. Weak lensing

Among the cosmological probes allowing the analysis of the nature of DE, the cosmological WL has been earning a fundamental role (see [23, 24, 25, 26] for a thorough review). In fact, next generation WL surveys will cover a significant fraction of the sky and observe galaxies at deeper redshift, making WL a powerful tool to study the properties of the Universe. Furthermore, WL tomography will allow to significantly increase the cosmological information that can be recovered from such surveys (see [27] and [28, 29, 30] for details about lensing tomography).

The power spectrum for the WL convergence between the  $i$ th- and  $j$ th- redshift bin is given by:

$$P_{(ij)}(\ell) = \left(\frac{H_0}{c}\right)^4 \int \frac{c dz}{H(z)} W_i(z) W_j(z) P_{\text{NL}}\left(\frac{\ell}{r(0, z)}, z\right). \quad (8)$$

Here  $P_{\text{NL}}(\ell/r(0, z), z)$  is the non-linear matter power spectrum, at the redshift  $z$  and wave number  $k = \ell/r(0, z)$ ; the quantity  $r(z, z_s)$  is the radial comoving distance between  $z$  and  $z_s$ ,

$$r(z, z_s) = \int_z^{z_s} \frac{c dz'}{H(z')}, \quad (9)$$

while

$$W_i(z) = \frac{3}{2} \Omega_{m0} F_i(z) (1+z) \quad (10)$$

is the window function which weights different redshift bins according to the factor  $F_i(z)$ ,

$$F_i(z) = \int_{Z_i} dz_s \frac{n_i(z_s) r(z, z_s)}{r(0, z_s)}, \quad (11)$$

being  $Z_i$  the  $i$ -th redshift bin. The function  $n_i(z)$  is the normalized redshift distribution of the source galaxies falling in the  $i$ -th photometric redshift bin, per unit solid angle,

$$n_i(z) = D_i(z) \left[ \int_0^\infty dz' D_i(z') \right]^{-1}, \quad (12)$$

where

$$D_i(z) = \int_{z_{ph}^{(i)}}^{z_{ph}^{(i+1)}} dz_{ph} n(z) p(z_{ph}|z). \quad (13)$$

The last expression codifies the effect of errors in photometric redshifts of source galaxies [31]. In fact, due to the large number of observed galaxies with future surveys, one needs

to refer to their photometric redshifts, even if the determination of these redshifts may be not so accurate as the spectroscopic ones. In the model given by (13), the mapping between the photometric  $z_{ph}$  and the spectroscopic redshift  $z$  is obtained convolving the overall galaxy distribution per unit solid angle,  $n(z)$ , with a probability distribution  $p(z_{ph}|z)$  in  $z_{ph}$  at a given  $z$ . We choose a Gaussian function at each redshift for the distribution of photometric redshifts, i.e.

$$p(z_{ph}|z) = \frac{1}{\sqrt{2\pi}\sigma_z} \exp\left[-\frac{(z - z_{ph})^2}{2\sigma_z^2}\right] \quad (14)$$

while the overall distribution of source galaxies is chosen to have the parametrized form:

$$n(z) = \frac{d^2N}{dz d\Omega} = \frac{B}{z_0 \Gamma\left(\frac{A+1}{B}\right)} \left(\frac{z}{z_0}\right)^A \exp\left[-(z/z_0)^B\right], \quad (15)$$

where  $A$ ,  $B$  and  $z_0$  are the parameters. One can easily check that equation (13) turns into:

$$D_i(z) = \frac{1}{2}n(z) [\text{erf}(x_{i+1}) - \text{erf}(x_i)], \quad (16)$$

with  $x_i \equiv (z_{ph}^{(i)} - z)/\sqrt{2}\sigma_z$  and  $\text{erf}(x)$  the error function.

The cosmic shear power spectrum will receive a shot-noise contribution from the random intrinsic ellipticities of source galaxies and measurement error [32]. Thus, the observed power spectrum between redshift bins  $i$  and  $j$  can be expressed as:

$$P_{(ij)}^{\text{obs}}(\ell) = P_{(ij)}(\ell) + \delta_{ij} \frac{\sigma_\epsilon^2}{\bar{n}_i} \quad (17)$$

where  $\sigma_\epsilon$  is the rms shear due to intrinsic ellipticity and measurement noise (we assume  $\sigma_\epsilon \simeq 0.22$  [27]) and

$$\bar{n}_i = \left[\frac{n_g}{a_{\text{min}}^{-2}}\right] \left(\frac{1}{60} \frac{\pi}{180}\right)^{-2} \hat{n}_i \quad (18)$$

is the average number density of galaxies per steradians in the  $i$ -th redshift bin,  $n_g$  being the number of galaxies per square arcminute and  $\hat{n}_i$  the fraction of sources belonging to the bin.

The covariance between the power spectra  $P_{(ij)}^{\text{obs}}(\ell)$  and  $P_{(mn)}^{\text{obs}}(\ell')$  is approximately given by

$$\text{Cov} [P_{(ij)}^{\text{obs}}(\ell), P_{(mn)}^{\text{obs}}(\ell')] = \frac{\delta_{\ell\ell'}}{(2\ell + 1)\Delta\ell f_{\text{sky}}} [P_{(im)}^{\text{obs}}(\ell) P_{(jn)}^{\text{obs}}(\ell') + P_{(in)}^{\text{obs}}(\ell) P_{(mj)}^{\text{obs}}(\ell')] \quad (19)$$

where  $f_{\text{sky}}$  is the sky fraction covered by the survey and  $\Delta\ell$  is the bin width centred at  $\ell$ . The above expression assumes that the power spectrum in each multipole bin is very flat, in order to replace the value of the spectrum evaluated at the bin center with the average of spectrum over each bin (see Appendix A for the complete expression). In addition, we have not included the non-Gaussian term, due to the contribution of the shear trispectrum [33, 34].

### 2.3. Fisher's formalism

The Fisher matrix formalism [35, 36, 37] provides lower limits to the error bars of the cosmological parameters one wishes to measure. The basic tool in Fisher's method is the likelihood function, yielding the probability that a model gives the set of data  $\mathbf{x}$ .

Suppose we want to test an hypothesis, *i.e.* a cosmological model set by  $M$  parameters  $\boldsymbol{\theta} = (\theta_1, \theta_2, \dots, \theta_M)$ . The likelihood function  $L(\mathbf{x}|\boldsymbol{\theta}) = \exp[-\mathcal{L}(\mathbf{x}|\boldsymbol{\theta})]$  is often a complicated function of  $\boldsymbol{\theta}$ ; the value  $\hat{\boldsymbol{\theta}}$  corresponding to the peak of  $L$  defines the *maximum likelihood estimator* which, in the limit of large data sets, becomes the *best unbiased estimator* of the actual parameter set. Thus, the likelihood can be Taylor expanded to second order (the first non-vanishing term) around  $\hat{\boldsymbol{\theta}}$ , being so approximated with a multivariate Gaussian distribution

$$L(\mathbf{x}|\boldsymbol{\theta}) \propto \exp\left(-\frac{1}{2}\Delta\boldsymbol{\theta}^T \mathbf{C}(\boldsymbol{\theta})^{-1} \Delta\boldsymbol{\theta}\right); \quad (20)$$

here

$$\mathbf{C}(\boldsymbol{\theta})^{-1} = \left. \frac{\partial^2 \mathcal{L}(\mathbf{x}|\boldsymbol{\theta})}{\partial\theta_\alpha \partial\theta_\beta} \right|_{\boldsymbol{\theta}=\hat{\boldsymbol{\theta}}} \quad (21)$$

is a positive semi-definite non-singular matrix, dubbed *covariance matrix* of the  $\theta_\alpha$ . We remind that Equation (20) holds just in a sufficiently small neighborhood around the maximum  $\hat{\boldsymbol{\theta}}$ . In turn, the *Fisher information matrix* reads

$$\mathbf{F}_{\alpha\beta}(\boldsymbol{\theta}) = \left\langle \frac{\partial \mathcal{L}(\mathbf{x}|\boldsymbol{\theta})}{\partial\theta_\alpha} \frac{\partial \mathcal{L}(\mathbf{x}|\boldsymbol{\theta})}{\partial\theta_\beta} \right\rangle_{\boldsymbol{\theta}=\hat{\boldsymbol{\theta}}} = \left\langle -\frac{\partial^2 \mathcal{L}(\mathbf{x}|\boldsymbol{\theta})}{\partial\theta_\alpha \partial\theta_\beta} \right\rangle_{\boldsymbol{\theta}=\hat{\boldsymbol{\theta}}}; \quad (22)$$

the average  $\langle \dots \rangle = \int \mathcal{L}(\mathbf{x}|\boldsymbol{\theta}) \dots d^N \mathbf{x}$  is taken over all possible data realizations, given the model parameters. The feature making Fisher's formalism so significant is the Cramér-Rao theorem. It states that the parameter variance about any unbiased estimator value owns a lower bound:  $\Delta\theta_\alpha \geq \sqrt{(\mathbf{F}^{-1})_{\alpha\alpha}}$ , if the other parameters are estimated from the data as well,  $\Delta\theta_\alpha \geq 1/\sqrt{\mathbf{F}_{\alpha\alpha}}$ , if all the other parameters are known. Therefore, the Fisher information matrix components are the expectation values of  $\mathbf{C}^{-1}(\hat{\boldsymbol{\theta}})$ . Accordingly, the inverse of the Fisher matrix is an estimate of the covariance matrix of the parameters  $\mathbf{C}(\boldsymbol{\theta}) \approx \mathbf{F}^{-1}$ .

A convenient way to re-write the Fisher matrix is computing the derivatives of the likelihood function using the following chain rule [38]:

$$\left. \frac{\partial \mathcal{L}(\mathbf{x}|\boldsymbol{\theta})}{\partial\theta_\alpha} \right|_{\boldsymbol{\theta}=\hat{\boldsymbol{\theta}}} = \sum_\ell \left. \frac{\partial \mathcal{L}(\mathbf{x}|\boldsymbol{\theta})}{\partial x_\ell} \right|_{\mathbf{x}=\mathbf{x}(\hat{\boldsymbol{\theta}})} \left. \frac{\partial x_\ell}{\partial\theta_\alpha} \right|_{\boldsymbol{\theta}=\hat{\boldsymbol{\theta}}} \quad (23)$$

Thus, the Fisher matrix (22) can be expressed as:

$$\mathbf{F}_{\alpha\beta}(\boldsymbol{\theta}) = \sum_{\ell\ell'} \frac{\partial x_\ell}{\partial\theta_\alpha} \frac{\partial x_{\ell'}}{\partial\theta_\beta} \left\langle -\frac{\partial^2 \mathcal{L}(\mathbf{x}|\boldsymbol{\theta})}{\partial x_\ell \partial x_{\ell'}} \right\rangle_{\mathbf{x}=\mathbf{x}(\hat{\boldsymbol{\theta}})} \quad (24)$$

$$= \sum_{\ell\ell'} \frac{\partial x_\ell}{\partial\theta_\alpha} \mathbf{F}_{\ell\ell'}(\boldsymbol{\theta}) \frac{\partial x_{\ell'}}{\partial\theta_\beta} \quad (25)$$

$$\approx \sum_{\ell\ell'} \frac{\partial x_\ell}{\partial\theta_\alpha} \mathbf{C}_{\ell\ell'}^{-1}(\boldsymbol{\theta}) \frac{\partial x_{\ell'}}{\partial\theta_\beta}, \quad (26)$$

where  $\mathbf{F}_{\ell\ell'}$  and  $\mathbf{C}_{\ell\ell'}$ , respectively, are the Fisher and the covariance matrix for the observables  $\mathbf{x}$ . The region in the  $M$ -dimensional space of the parameters, defined by  $Q(\theta, \hat{\theta}) = \Delta\theta_\alpha^T \mathbf{F}_{\alpha\beta} \Delta\theta_\beta = K^2$ , is a hyper-ellipsoid of constant probability density for the function (20). Marginalizing over the other parameters, one can project this ellipsoid in the two-parameter subspace, yielding a two-dimensional ellipse. The analytical expression for the projected ellipse for the two parameters  $\theta_\alpha$  and  $\theta_\beta$  is given by [39]:

$$\begin{pmatrix} \Delta\theta_\alpha & \Delta\theta_\beta \end{pmatrix} \begin{bmatrix} (\mathbf{F}^{-1})_{\alpha\alpha} & (\mathbf{F}^{-1})_{\alpha\beta} \\ (\mathbf{F}^{-1})_{\alpha\beta} & (\mathbf{F}^{-1})_{\beta\beta} \end{bmatrix}^{-1} \begin{pmatrix} \Delta\theta_\alpha \\ \Delta\theta_\beta \end{pmatrix} = \Delta\chi^2(N=2, \sigma) \quad (27)$$

This can be interpreted as an estimate of the confidence region within a given confidence level  $\sigma$  for the two parameters  $\theta_\alpha$  and  $\theta_\beta$ .

### 3. Forecasts for Future Experiments

We present here the results of the Fisher analysis of future experiments, considering both WL and CMB measurements. For definiteness we assume a fiducial WL survey with characteristics similar to those of the recently proposed DUNE project [40]. We assume a redshift distribution of the form (15) with  $A = 2$ ,  $B = 1.5$  and  $z_0 \simeq z_m/1.412$ , corresponding to a median redshift of the survey  $z_m = 0.9$  (see [27]), and a mean surface density of galaxies  $n_g = 35 \text{ arcmin}^{-2}$ . The full survey, covering half of the sky ( $f_{sky} = 0.5$ ), is divided into  $N = 5$  redshift bins, with  $p(z_{ph}|z)$  given by equation (14) and  $\sigma_z(z) = 0.05(1+z)$ .

We consider lensing multipoles up to  $\ell_{\max} = 20000$ , since we find that results do not depend significantly on larger  $\ell$ . However, one should bear in mind that when considering scales  $\ell \gg 1000$  there could be some non-linear and baryonic effects on the matter power spectrum, and so on the WL spectrum [41]. These effects, not yet well understood, could be important for forecasts. However, in this work we suppose these effects to be negligible.

For CMB data, we consider an ideal experiment with characteristics based on the 143GHz PLANCK channel: angular resolution  $\theta_{\text{fwhm}} = 7.1'$  and sensitivity  $\sigma_T = 42\mu\text{K arcmin}$ ,  $\sigma_P = 80\mu\text{K arcmin}$ .

The cosmological model we consider is characterized by 7 parameters with fiducial values:

$$\vec{\theta} = \{ \omega_b = (0.045 \cdot 0.7^2), \omega_m = (0.30 \cdot 0.7^2), \Omega_m = 0.30, n_s = 1.00, \sigma_8 = 0.8, \Lambda_{\text{DE}} = 5 \cdot 10^{-3} \text{GeV}, \beta = 0.1 \}.$$

Here  $\Omega_m$  represents the current total (CDM + baryons) matter density in units of the critical density;  $\omega_b \equiv \Omega_b h^2$  and  $\omega_m \equiv \Omega_m h^2$  are the physical baryons and total matter densities, respectively;  $n_s$  is the slope of the primordial power-law spectral index of density fluctuations;  $\sigma_8$  is the rms mass fluctuation in spheres of  $8h^{-1}$  Mpc radius while  $\Lambda_{\text{DE}}$  and  $\beta$  were defined in Sec. 2.1. Let us notice that the class of DE models considered here reduces to  $\Lambda\text{CDM}$  for  $(\Lambda_{\text{DE}})^4 \simeq 10^{-47} \text{GeV}^4$  and  $\beta = 0$ . Moreover, the fiducial values



**Table 1.** Estimated errors on model parameters.

	CMB		WL		WL+CMB	
	SUGRA	SUGRA	SUGRA	SUGRA	SUGRA	SUGRA
	$\beta = 0.$	$\beta = 0.1$	$\beta = 0.$	$\beta = 0.1$	$\beta = 0.$	$\beta = 0.1$
$100*\omega_b$	0.016	0.019	0.5	0.9	0.011	0.012
$\omega_m$	0.002	0.006	0.016	0.03	0.0004	0.0005
$\Omega_m$	0.05	0.12	0.002	0.0014	0.0011	0.0014
$n_s$	0.004	0.005	0.012	0.018	0.0014	0.0021
$\sigma_8$	0.07	0.13	0.0026	0.0029	0.0017	0.0016
$\lambda$	7.2	9.5	0.89	1.1	0.28	0.28
$\beta$	–	0.04	–	0.018	–	0.0016
$\tau$	0.005	0.006	–	–	–	–

of DE parameters  $\Lambda_{de} = 5 \cdot 10^{-3} \text{GeV}$  and  $\beta = 0.1$  are chosen in order to reproduce at  $z = 0$  an effective equation of state which mimics the case of  $\Lambda$ CDM model,  $w = -0.95$ . Finally, when dealing with CMB data, we also need to fix the value of the optical depth to reionization,  $\tau = 0.10$ .

We compute the CMB anisotropies (temperature and polarisation) power spectra and the transfer functions, used to calculate linear matter power spectrum, using a modified version of CAMB [42]. To evaluate the non-linear matter power spectrum,  $P_{NL}$ , we employ the prescription by Smith *et al.* [43]. This is only tested for model with a cosmological constant; as we are concerned here with Fisher matrix estimates assume that the results of [43] can be extended to coupled models simply by taking into account the non-standard scaling of  $\rho_c$  (eq. 3). Numerical derivatives were evaluated considering a 5% stepsize, except for  $\Lambda_{DE}$ , where we adopted a 5% stepsize on  $\lambda \equiv \text{Log}_{10}(\Lambda_{DE}/\text{GeV})$ .

### 3.1. CMB measurements

Table 1 lists the estimated errors on the various parameters considered. For each data set, we compare forecasts for the target model with results for a SUGRA model with the same values of the relevant parameters. The table clearly shows that a PLANCK-like experiment is able to provide a measurement of a direct DE-DM interaction at 68% confidence level, even for moderate values of the coupling strength  $\beta$ . However, we expect that at 90% confidence level data will still be compatible with  $\beta = 0$ .

In any case, allowing for a direct interaction strongly degrades the experimental sensitivity on the parameters characterizing the matter density and the normalization of the primordial spectrum of density fluctuations. Errors on these quantities increase by a significant amount.

Figure 2 shows the joint 68% confidence regions between  $\beta$  and each of the other parameters, except for  $\tau$ , considering only CMB data. In each plot we marginalized over the parameters not shown.  $\beta$  is strongly correlated with most parameters considered here, with the exception of  $\omega_b$  (and  $\tau$ ), thus introducing additional degeneracies in actual

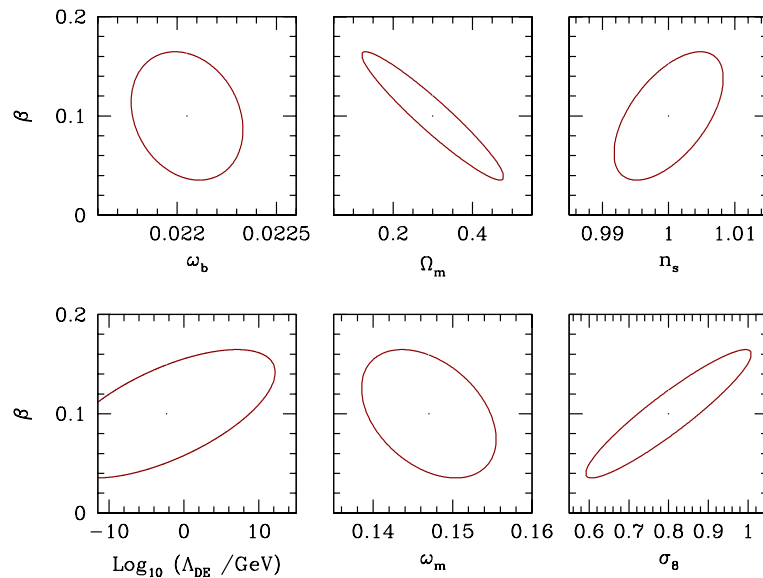


**Figure 2.** Forecasts of joint  $1\text{-}\sigma$  confidence regions on the coupling parameter  $\beta = 0.1$  and selected parameters, for a PLANCK-like experiments, after full marginalization over the remaining parameters.

data analysis.

A detailed characterization of these degeneracies would require a different approach than that followed here (e.g. Monte Carlo Markov Chains simulations). We just point out that they can be understood recalling that the heights of the acoustic peaks of CMB spectra are sensitive to the total matter density and to baryon/dark matter ratio at last scattering. In coupled models, these quantities are not univocally determined by their present day value, but strongly depend on  $\beta$ . In addition, the total growth between the last scattering epoch and today is strongly sensitive to  $\beta$ , resulting in a clear degeneracy between  $\beta$  and  $\sigma_8$ .

Let us notice that, as we are concerned with a combination of CMB and WL data, the parameter set is not optimized for CMB experiments. Using a different parametrisation can alter error estimates and/or the degeneracies between the various parameters. In particular, CMB data are better described in terms of the angle subtended by the acoustic horizon at recombination,  $\theta$ , and the amplitude of the primordial spectrum of density fluctuations  $A_s$ , rather than in terms of  $\Omega_m$  and  $\sigma_8$ . This results in large errors on the latter parameters, when CMB data alone are considered. Adopting a set of parameters better suited to the analysis of CMB data results in slightly lower error estimates overall, but the effects of coupling are largely unchanged.

### 3.2. Weak Lensing

Figure 3 is analogous to figure 2 for our target weak lensing survey. Together with Table 1, these results show the great potential of WL surveys in constraining interacting DE models. Marginalized errors on  $\beta$  and  $\lambda$  are of the order of  $\sigma(\beta) \simeq 0.02$  and

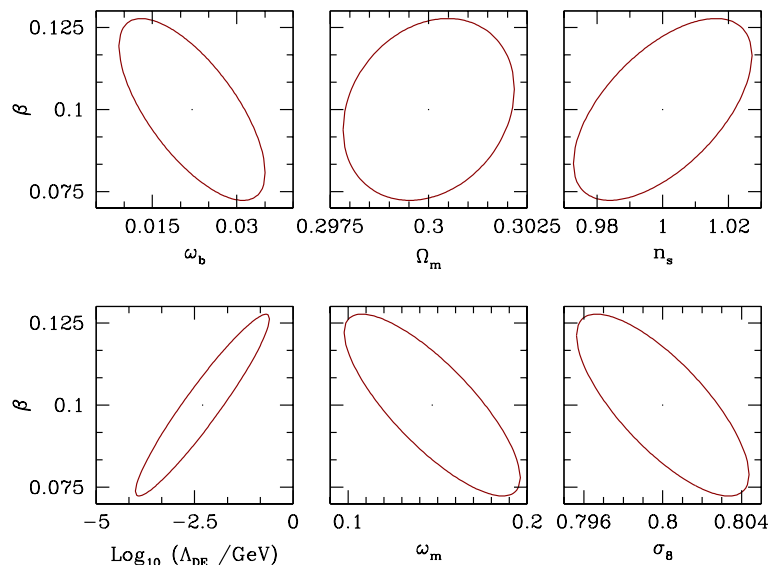


**Figure 3.** Forecasts of joint  $1\text{-}\sigma$  confidence regions on the coupling parameter  $\beta = 0.1$  and selected parameters, for a DUNE-like experiments, after full marginalization over the remaining parameters. Notice the change of scales with respect to figure 2

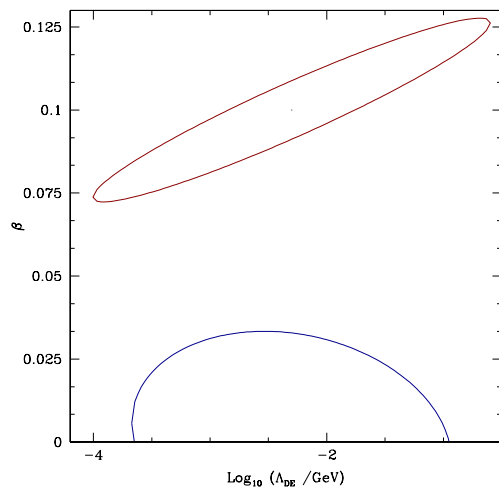


**Figure 4.** Comparison between the  $1\text{-}\sigma$  confidence regions of a coupled SUGRA model with  $\beta = 0.1$  (red) and a non-coupled SUGRA model with  $\beta = 0$  (blue) for a WL experiment. It is clearly possible to distinguish between the two models.

$\sigma(\lambda) \simeq 1$ ; these figures represent a factor of 2, or more, improvement over Planck estimates. WL data alone can clearly distinguish the target model from a non-coupled model or a cosmological constant even at the  $3\sigma$ -level, *viceversa* assuming a reference SUGRA model with  $\beta = 0$ , we can expect to put an upper limit  $\beta \lesssim 0.03$ , at the same confidence level (see figure 4).

As expected, WL surveys perform significantly better than CMB experiments also with respect to parameters specifying the current matter density,  $\Omega_m$  and  $\sigma_8$ . Moreover, constraints on these parameters are not significantly affected by the coupling degrees

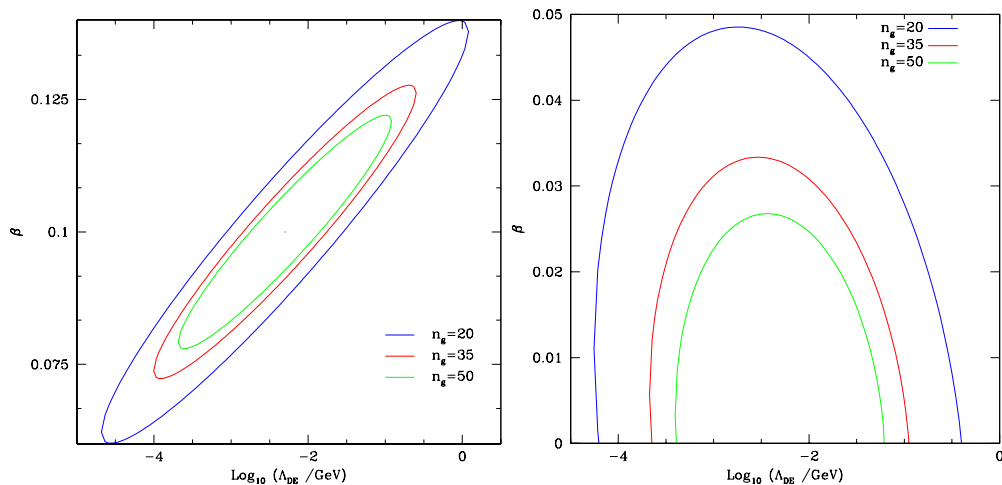


**Figure 5.** Joint  $1\text{-}\sigma$  confidence regions on  $\beta$  and  $\Lambda_{\text{DE}}$  after marginalization over the remaining parameters, for different number of galaxies  $n_g$ . On the left SUGRA coupled model with  $\beta = 0.1$ , on the right SUGRA coupled model with  $\beta = 0$  and  $\beta$  derivatives calculated only on one side, for positive values of the parameter.

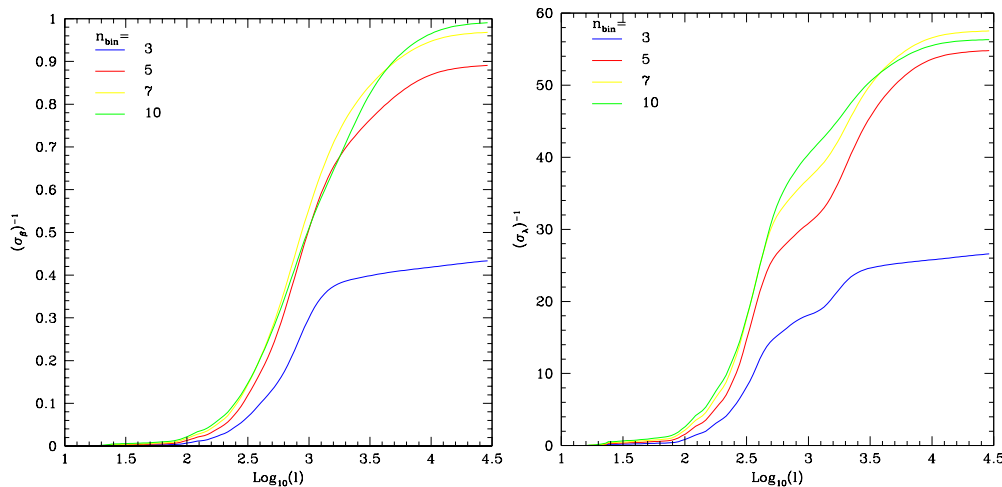


**Figure 6.** Inverse error as a function of the maximum multipole for the WL survey, for different numbers of redshift bins. Left panes show results for  $\beta$ , right panel refers to  $\lambda$ .

of freedom. Errors on the remaining parameters, instead, increase by a factor of  $\sim 2$ . Finally, we consider a combination of CMB and WL data. CMB and WL probe very different epoch of the Universe and are sensitive to different combination of cosmological parameters. Considering both CMB and WL data allows to constrain the DE parameters with a few percent accuracy, and significantly reduces the degeneracies introduced by DE coupling. In this case, the errors on the cosmological parameters are very similar in both models considered, with the exception of  $n_s$ .

Next we considered how our results depend on the characteristic assumed for the target survey. In figure 5 the impact of mean surface density of galaxies on the

determination of  $\beta$  and  $\lambda$ . With  $n_g = 25 \text{ arcmin}^{-2}$  constraints on  $\beta$  degrades by  $\sim 50\%$ , while  $n_g = 50 \text{ arcmin}^{-2}$  gives only a marginal improvement on expected errors; constraints on  $\lambda$  are similarly affected. However, even in the worst case considered here, next generations WL survey will provide an improvement over the information that we are likely to obtain from PLANCK data.

Lastly, we consider the dependence of our results on the number of bins and the multipoles range considered. In figure 6 we plot the inverse of the expected variance on  $\beta$  and  $\lambda$  as a function of the maximum multipole considered in the analysis and for different number of bins. With 3 redshift bins, the precision on both parameters depends mostly on multipole up to a few thousands; smaller scales do not provide a significant contribution. Dividing the survey in 5 bins strongly improves the constraints on both parameters and allows to exploit information from multipoles up to  $\sim 10000$ . For a DUNE-like survey, a further increase in the number of bins does not lead to significant improvements on the constrains on coupled models parameters.

It must be outlined that these results assume that the theoretical framework used to predict the matter power spectrum on intermediate ( $1h\text{Mpc}^{-1} \lesssim k \lesssim 20h\text{Mpc}^{-1}$ ) and small ( $k > 20h\text{Mpc}^{-1}$ ) scales can accurately account for the effects of baryons on non-linear structures. In general, the fitting formulas used to predict the non-linear power spectrum are calibrated using dissipationless N-body simulations and, therefore, do not properly describe baryonic structures. While baryons make up  $\simeq 15-20\%$  of the matter in the Universe and on large scales are expected to trace the DM field, their distribution inside halos is significantly different from DM. In turn, this alters the shape of the non-linear power spectrum on the corresponding scales, and the possibility of extracting precision constraints from  $P_{\text{NL}}(k)$  hinges on our capability of accurately modeling baryon physics [41]. However, simulations do not yet have the accuracy required for precision constraints and the problem is even more serious for the coupled models considered in this work. Modelling non linear stages though spherical growth, Mainini [44] shew that baryons and DM will be however differently distributed, even independently of the onset of gas dynamics. N-body simulations of cDE models were performed [45], by using a Ratra-Peebles [46] potential; hydro simulations, instead, were never produced. Should accurate prediction be still unavailable for the analysis of a DUNE-like experiment, a more conservative cutoff of  $l \simeq 1000$  would be required. Figure 6 shows that in this case the expected errors on  $\Lambda$  and  $\beta$  would increase by a factor  $\sim 2$ .

#### 4. Discussion

All previous analysis shows that, even if we admit quite a little DM-DE coupling, we open a Pandora's box, leading to a severe degradation in our capacity to deduce cosmological parameters from a given set of measures.

As a matter of fact, coupling destroys our trust that the period between the recombination and the start of DE relevance is under control. If coupling is absent, during such period  $\Lambda\text{CDM}$  is a fair approximation. Let us then remind what happens

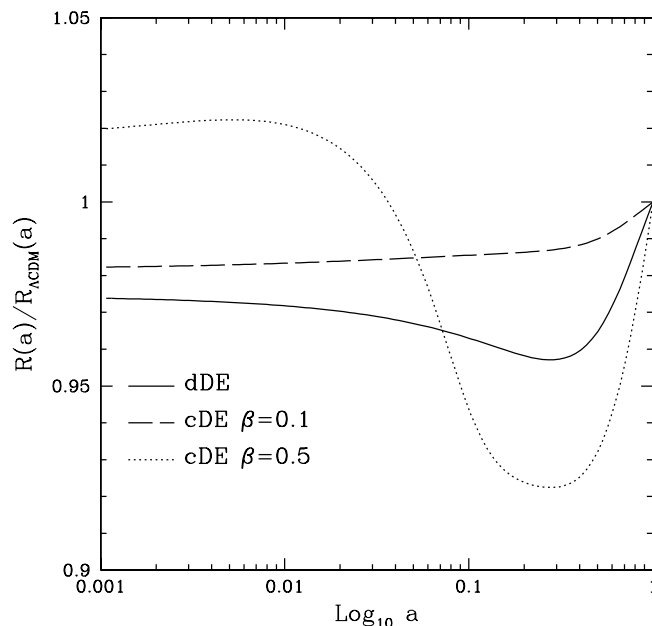


**Figure 7.** Scale dependence of comoving distances in coupled or uncoupled SUGRA cosmologies, compared with  $\Lambda$ CDM. The case  $\beta = 0.5$ , corresponding to a rather strong DM–DE coupling is also shown.

to the growth factor, as soon as coupling is onset: Figure 1 shows that: (i) deviations from SCDM are significant already when  $a \sim 0.02$ ; (ii) they are then different for DM and baryons; (iii) they work in the opposite direction, in respect to the effects of a DE components.

As far as the growth factor is concerned, a tiny coupling is able to overwhelm a huge DE amount, with compensation occurring for  $a \sim 0.3$ – $0.4$ , however keeping always  $g(a)$  at values greater by  $\sim 10$ – $15\%$ . Altogether, growth is faster in coupled models. Hence, if we do not include the information that coupling is zero in the fit, we can find an agreement between data and a wider range of DE amounts.

Similar points can be made for the comoving radial distance  $R(z) \equiv r(0, z)$  (see eq. 9). In Figure 7 we compare comoving distances for  $\Lambda$ CDM with various cosmologies. The Figure shows that dDE, in the absence of other parameter shifts, sets the Last Scattering Band (LSB) closer to the observer. Once again, a mild coupling acts in the opposite direction and tends to re-set the LSB at the distance it had in  $\Lambda$ CDM. In the Figure we consider the behavior of distances also for a rather strong coupling,  $\beta = 0.5$ . Then the distance behavior is different in the period when DE density can be neglected, in respect to the epoch when DE and DM have similar densities. The key point, however, is that the LSB becomes then farther from the observer. When fitting CMB data to such models, in order to compensate such effect, the value of  $H_o$  tends to be increased. Strong coupling therefore yields a large Hubble parameter estimate.

Figures 8 finally show the scale dependence of the density parameters in the different models. Once again, when DE is mildly coupled, a behavior more similar to  $\Lambda$ CDM is

recovered. On the contrary, when considering a greater coupling strength, we see that DE and DM keep similar densities up to a fairly large redshift. This was indeed the initial motivation of cDE cosmologies.

Altogether, these Figures indicate that adding a small coupling reduces the effects of the very passage from  $\Lambda$ CDM to dDE; owing to the excellent fit that  $\Lambda$ CDM cosmologies have with data, this tells us that only highly refined CMB data will be able to test the possibility that a mild DM–DE coupling exists.

On the contrary, a stronger coupling, although easing the coincidence problem, displaces several observables in a unacceptable way.

## 5. Summary and Conclusions

Future WL surveys will certainly put more stringent constraints on cosmological parameters and will be crucial to break quite a few degeneracies between parameters.

Within this context, in this paper we focus on coupled DE models with a twofold aim. Detecting a signal of DM–DE coupling would be certainly decisive to fix the nature of the dark components. Henceforth determining the level of sensitivity needed to appreciate such an effect is crucial in setting the appeal of forthcoming projects. There is however a complementary aspect which deserves much attention. In order to convert raw data into physical information, a set of parameters, spanning a variety of models, is to be fixed; a bias on parameter selection, however, can lead to an optimistic estimate of the confidence level for the best fitting model, far from reality.

In this paper, we focused on this kind of danger, when we open the option of DM–DE coupling. Even if such coupling is absent or quite weak, we showed that just considering its possibility may widen the error bars for a number of parameters, also apparently unrelated to the coupling itself. In a sense, when a new degree of freedom is opened, such an effect is natural and expected. Coupling, however, has really a major impact, affecting different parameters for the different observables considered here; moreover, its impact is drastically reduced when we work out parameter values by using simultaneously both observables.

Before outlining our main conclusions it is however worth reminding a technical limit we had to face. While CMB predictions depend on linear spectra, the WL spectrum is limited to its non-linear shape. For the purpose of the present analysis, we assumed that prescription for  $\Lambda$ CDM models [43] can be trivially extrapolated to coupled models, so enabling us to estimate the non linear spectrum once the linear spectrum is known. Let us however remark that the shift was estimated from quite a wide set of  $\Lambda$ CDM simulations. Simulations of cosmological models with state parameters  $w \neq 1$ , although performed by several authors, are still not so extensively studied as  $\Lambda$ CDM; let alone coupled DE simulations: in this case the only available simulations are due to [45] and deal with a potential  $V(\phi)$  different from SUGRA.

However, differences between prescriptions for  $\Lambda$ CDM and dDE are small [47] and it seems however clear that model differences can most affect the rate of evolution of halo

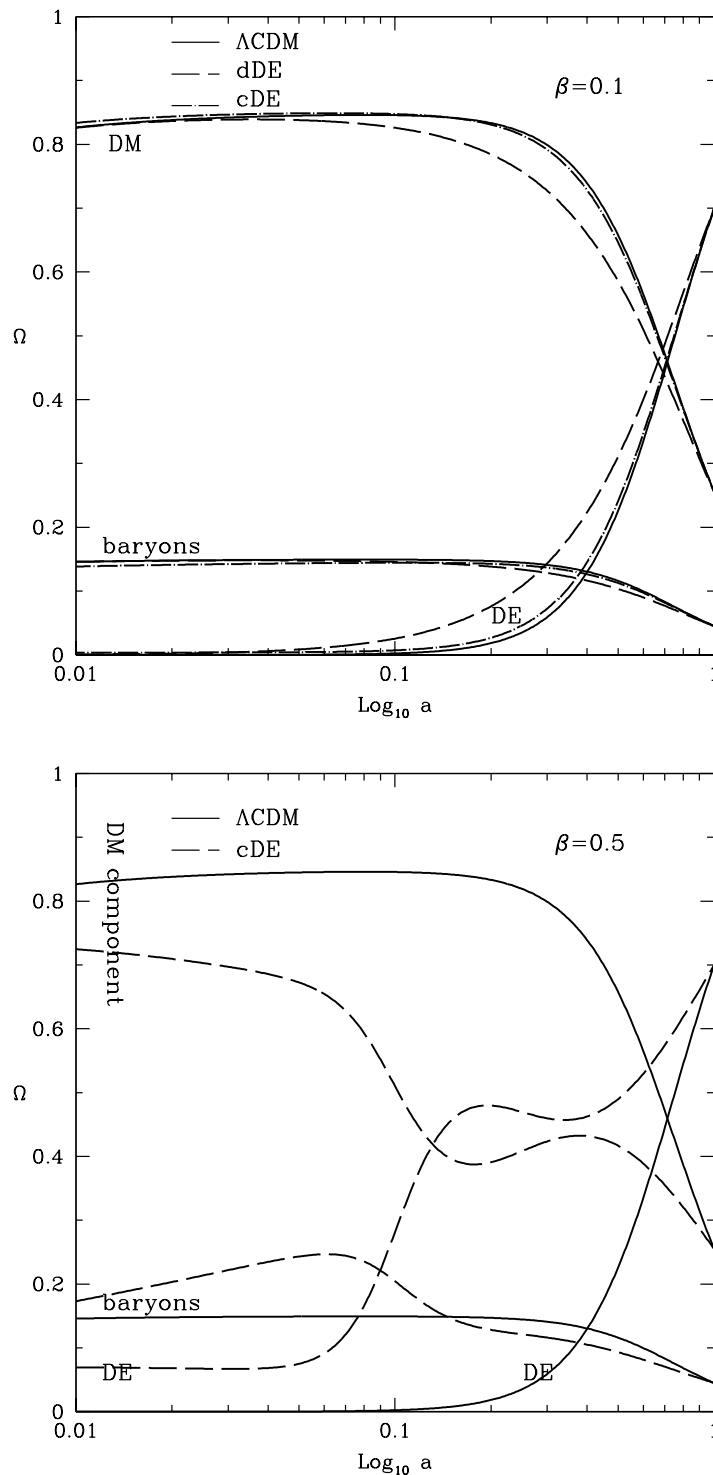


**Figure 8.** Scale dependence of the density parameters of the various components in  $\Lambda$ CDM, compared with other models. In the upper panel uncoupled and weakly coupled SUGRA models are considered. For the sake of comparison, in the lower panel we also show the effects of choosing a stronger coupling.

concentration, slightly shifting the scale where non-linearity effects become significant. The use of more precise prescriptions can therefore only cause minor variation on the



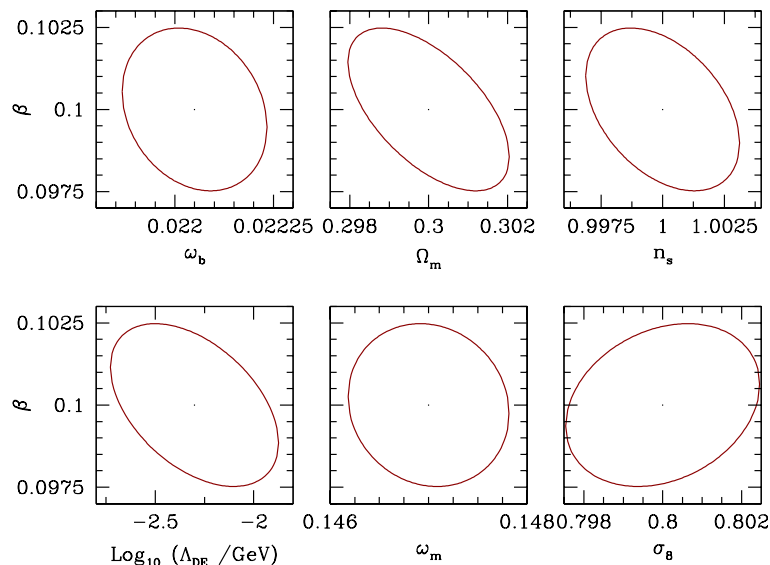


**Figure 9.** Forecasts of joint  $1\text{-}\sigma$  confidence regions on the coupling parameter  $\beta = 0.1$  and selected parameters, for a combination of a PLANCK-like and a DUNE-like experiment, after full marginalization over the remaining parameters.

estimated errors and, although welcome, such simulations are not expected to interfere substantially with our conclusions.

Our estimates were based on assuming that a photometric survey is available, with  $\sigma_z(z) = 0.05(1+z)$  and a median redshift  $z_m = 0.9$ , covering half of the sky ( $f_{sky} = 0.5$ ). These features are similar to the recently proposed DUNE experiment [40]. We also compared and combined results from WL with the constraints expected for an ideal Planck-like experiment. The basic results of our calculations are quoted in table 1 which is one of the main results of this work.

A first set of conclusions concerns an ideal CMB experiment considered by itself. In this case, introducing coupling degrees of freedom is crucial for the error estimates on some of parameters, also apparently unrelated to coupling. In particular, while the error on  $\omega_b$  keeps  $\sim 1\%$ , the errors on  $\omega_m$  and  $\sigma_8$  increase from 1.3% to 3.9% and from 9% to 16%, respectively.

From a physical point of view, the option opened by coupling is that expansion rate and fluctuation growth, from the last scattering band to the observer's site, is non-standard (*e.g.*, the proportionality law  $\rho_m \propto a^{-3}$  could be mildly violated). Although CMB data themselves set stringent limits on such deviations, this widens the volume of the parameter space consistent with a given data set; in particular, it increases the likelihood of values of  $H_0$  that would otherwise be negligible and, because of the intercorrelation amongst parameters, this reflects immediately on  $\omega_m$  and  $\Omega_m$  estimates.

Similar effects occur in WL experiments, although involving different parameters. Such experiments are a direct test of  $\Omega_m$ , whose estimated error is reduced by a factor  $> 30$  in respect to a CMB experiment. When the coupling option is opened, the error

on  $\Omega_m$  does not increase; on the contrary, it becomes easier to attribute raw data uncertainties to other parameters and, although marginally, the error on  $\Omega_m$  becomes somehow smaller.

A completely new situation occurs if both CMB and WL measurements are simultaneously used. In this case, the opening of the coupling option causes just a marginal increase of the errors on most parameters. This is a clear indication of the complementarity of the CMB and WL measurements, as described in [48] and one of our conclusion is that the combination of these observables, besides of providing parameter values independent of  $\beta$ , can set a (nearly-)final word on the coupling option.

As a matter of fact, by comparing figure 2, figure 3 and figure 9, we see that, when joining CMB and WL results, the degeneracies, between  $\beta$  and  $\sigma_8$ , as well as between  $\beta$  and  $\Omega_m$ , disappear. Breaking degeneracies is the main aim when different observables are simultaneously considered. We see that, from this point of view, the efficiency of using both CMB and WL measures can be hardly overestimated.

Let us then focus on the case of the spectral index of scalar fluctuations. When both CMB and WL data are used to constrain  $n_s$ , a sharp reduction of errors occurs. No surprise that CMB data, by themselves, reflecting the state of the universe before the onset of non linear processes, were more efficient to constrain  $n_s$ , with or without coupling, than WL measures. Joining together the two observables, we then see errors to decrease from 0.4% and 1.2% down to 0.16%, in the uncoupled case; in the presence of coupling we have a similar behavior, with errors passing from 0.5% and 1.8% down to 0.25%. The error level achieved, in both cases, is exceptional, even for precision cosmology, and clearly suggests to relieve the constraint of a single  $n_s$  value, so inspecting its possible scale dependence, with realistic possibilities to find a direct insight into the nature of the inflationary potential.

In conclusion, future WL surveys could really allow a significant step forward in the comprehension of the dark cosmic side; we can affirm that, when they will be available, the endeavour to put the genie back inside the lamp will approach a full success.

## Acknowledgments

LPLC is supported by NASA grant NNX07AH59G and JPL–Planck subcontract no. 1290790. We acknowledge the use of the CAMB package. LPLC and GLV thank S. Bonometto for insightful discussion and help with the preparation of the manuscript.

## Appendix A. Convergence power spectrum covariance

In order to determine the convergence power spectrum covariance, one can introduce the so called “flat-sky” approximation and treat the sky as flat, replacing spherical harmonic sums with Fourier transforms (FT). Of course, this approximation is acceptable just for small angular scales. We also consider the tomographic case and use Greek letters as superscripts to denote quantities belonging to different redshift bins. The FT of the

convergence field can be defined as:

$$\kappa^\alpha(\mathbf{l}) = \int d^2\boldsymbol{\theta} \kappa^\alpha(\boldsymbol{\theta}) \exp(-i\boldsymbol{\theta} \cdot \mathbf{l}), \quad (\text{A.1})$$

while the convergence power spectrum and trispectrum are, respectively:

$$\langle \kappa^\alpha(\mathbf{l}_1) \kappa^\beta(\mathbf{l}_2) \rangle = (2\pi)^2 \delta_D(\mathbf{l}_1 + \mathbf{l}_2) P_l^{\alpha\beta}, \quad (\text{A.2})$$

$$\langle \kappa^\alpha(\mathbf{l}_1) \dots \kappa^\delta(\mathbf{l}_4) \rangle_c = (2\pi)^2 \delta_D(\mathbf{l}_1 + \dots + \mathbf{l}_4) T^{\alpha\beta\gamma\delta}(\mathbf{l}_1, \mathbf{l}_2, \mathbf{l}_3, \mathbf{l}_4); \quad (\text{A.3})$$

here  $\delta_D$  is the Dirac function. The value of the lensing power spectrum in correspondence of a multipole  $l$  can be estimated as the mean over a multipole bin of width  $\Delta l$ , centered at  $l$ :

$$\mathcal{P}_l^{\alpha\beta} = \frac{1}{A} \int_{s_l} \frac{d^2\mathbf{l}_1}{A_l} \kappa^\alpha(\mathbf{l}_1) \kappa^\beta(-\mathbf{l}_1), \quad (\text{A.4})$$

where  $A_l = \int_{s_l} d^2\mathbf{l} \cong 2\pi l \Delta l$  is the area of the shell of width  $\Delta l$  corresponding to  $l$ , while  $A = 4\pi f_{sky}$  is the area of the survey. Quite in the same way, for the trispectrum we have:

$$\mathcal{T}_{ll'}^{\alpha\beta\gamma\delta} = \int_{s_l} \frac{d^2\mathbf{l}_1}{A_l} \int_{s_{l'}} \frac{d^2\mathbf{l}_2}{A_{l'}} T^{\alpha\beta\gamma\delta}(\mathbf{l}_1, -\mathbf{l}_1, \mathbf{l}_2, -\mathbf{l}_2). \quad (\text{A.5})$$

Let us then consider the following expression:

$$\langle \mathcal{P}_l^{\alpha\beta} \mathcal{P}_{l'}^{\gamma\delta} \rangle = \frac{1}{A^2} \int_{s_l} \frac{d^2\mathbf{l}_1}{A_l} \int_{s_{l'}} \frac{d^2\mathbf{l}_2}{A_{l'}} \langle \kappa^\alpha(\mathbf{l}_1) \kappa^\beta(-\mathbf{l}_1) \kappa^\gamma(\mathbf{l}_2) \kappa^\delta(-\mathbf{l}_2) \rangle. \quad (\text{A.6})$$

The 4-point function at the r.h.s. can be decomposed in its connected parts:

$$\begin{aligned} \langle \kappa^\alpha(\mathbf{l}_1) \kappa^\beta(-\mathbf{l}_1) \kappa^\gamma(\mathbf{l}_2) \kappa^\delta(-\mathbf{l}_2) \rangle &= \langle \kappa^\alpha(\mathbf{l}_1) \kappa^\beta(-\mathbf{l}_1) \kappa^\gamma(\mathbf{l}_2) \kappa^\delta(-\mathbf{l}_2) \rangle_c + \\ &+ \langle \kappa^\alpha(\mathbf{l}_1) \kappa^\beta(-\mathbf{l}_1) \rangle \langle \kappa^\gamma(\mathbf{l}_2) \kappa^\delta(-\mathbf{l}_2) \rangle + \\ &+ \langle \kappa^\alpha(\mathbf{l}_1) \kappa^\gamma(\mathbf{l}_2) \rangle \langle \kappa^\beta(-\mathbf{l}_1) \kappa^\delta(-\mathbf{l}_2) \rangle + \langle \kappa^\alpha(\mathbf{l}_1) \kappa^\delta(-\mathbf{l}_2) \rangle \langle \kappa^\gamma(\mathbf{l}_2) \kappa^\beta(-\mathbf{l}_1) \rangle. \end{aligned} \quad (\text{A.7})$$

Replacing their expression in eq. (A.6), one can easily recognize the contribution of the trispectrum, using eq. (A.3):

$$\begin{aligned} \langle \mathcal{P}_l^{\alpha\beta} \mathcal{P}_{l'}^{\gamma\delta} \rangle &= \frac{1}{A^2} \int_{s_l} \frac{d^2\mathbf{l}_1}{A_l} \int_{s_{l'}} \frac{d^2\mathbf{l}_2}{A_{l'}} (2\pi)^2 \delta_D(\mathbf{0}) T^{\alpha\beta\gamma\delta}(\mathbf{l}_1, -\mathbf{l}_1, \mathbf{l}_2, -\mathbf{l}_2) + \langle \mathcal{P}_l^{\alpha\beta} \rangle \langle \mathcal{P}_{l'}^{\gamma\delta} \rangle + \\ &+ \frac{1}{A^2} \int_{s_l} \frac{d^2\mathbf{l}_1}{A_l} \int_{s_{l'}} \frac{d^2\mathbf{l}_2}{A_{l'}} \langle \kappa^\alpha(\mathbf{l}_1) \kappa^\gamma(\mathbf{l}_2) \rangle \langle \kappa^\beta(-\mathbf{l}_1) \kappa^\delta(-\mathbf{l}_2) \rangle + \end{aligned} \quad (\text{A.8})$$

$$+ \frac{1}{A^2} \int_{s_l} \frac{d^2\mathbf{l}_1}{A_l} \int_{s_{l'}} \frac{d^2\mathbf{l}_2}{A_{l'}} \langle \kappa^\alpha(\mathbf{l}_1) \kappa^\delta(-\mathbf{l}_2) \rangle \langle \kappa^\gamma(\mathbf{l}_2) \kappa^\beta(-\mathbf{l}_1) \rangle, \quad (\text{A.9})$$

where  $(2\pi)^2 \delta_D(\mathbf{0}) = A$ . Owing to the definition of covariance,

$$\text{Cov} \left[ \mathcal{P}_l^{\alpha\beta}, \mathcal{P}_{l'}^{\gamma\delta} \right] \equiv \langle \mathcal{P}_l^{\alpha\beta} \mathcal{P}_{l'}^{\gamma\delta} \rangle - \langle \mathcal{P}_l^{\alpha\beta} \rangle \langle \mathcal{P}_{l'}^{\gamma\delta} \rangle, \quad (\text{A.10})$$

and using (A.2), one can then argue that the integrals in (A.8) make sense only if they correspond to the same  $l$ -bin; the same can be claimed for (A.9). This property can

be described introducing a Kronecker delta function  $\delta_{ll'}$ . Thus, the expression (A.10) becomes:

$$\begin{aligned} \text{Cov} \left[ \mathcal{P}_l^{\alpha\beta}, \mathcal{P}_{l'}^{\gamma\delta} \right] &= \frac{1}{A} \mathcal{T}_{ll'}^{\alpha\beta\gamma\delta} + \delta_{ll'} \frac{(2\pi)^2}{A^2} \int_{s_l} \frac{d^2 \mathbf{l}_1}{A_l^2} \left[ P_{l_1}^{\alpha\gamma} \langle \kappa^\beta(-\mathbf{l}_1) \kappa^\delta(\mathbf{l}_1) \rangle + P_{l_1}^{\alpha\delta} \langle \kappa^\gamma(\mathbf{l}_1) \kappa^\beta(-\mathbf{l}_1) \rangle \right] \\ &= \frac{1}{A} \left\{ \mathcal{T}_{ll'}^{\alpha\beta\gamma\delta} + \delta_{ll'} \frac{(2\pi)^2}{A_{s_l}} \int_{s_l} \frac{d^2 \mathbf{l}_1}{A_{s_l}} \left[ P_{l_1}^{\alpha\gamma} P_{l_1}^{\beta\delta} + P_{l_1}^{\alpha\delta} P_{l_1}^{\gamma\beta} \right] \right\} \end{aligned} \quad (\text{A.11})$$

$$\approx \frac{1}{4\pi f_{sky}} \mathcal{T}_{ll'}^{\alpha\beta\gamma\delta} + \frac{\delta_{ll'}}{2l\Delta l f_{sky}} \left[ P_l^{\alpha\gamma} P_l^{\beta\delta} + P_l^{\alpha\delta} P_l^{\gamma\beta} \right]. \quad (\text{A.12})$$

In the last line, we have supposed the lensing power spectrum to be smooth enough to treat it as a constant within each bin width.

## References

- [1] Riess A G, Kirshner R P, Schmidt B P, Jha S, et al. 1998 *Astrophys. J.* **116** 1009; Perlmutter S, Aldering G, Goldhaber G, et al. 1999 *Astrophys. J.* **517** 565; Riess A G, Strolger L-G, Tonry J, et al. 2004 *Astrophys. J.* **607** 665
- [2] de Bernardis P, Ade P A R, Bock J J, et al. 2000 *Nature* **404** 955; Padin S, Cartwright J K, Mason B S, et al. 2001 *Astrophys. J.* **549** L1; Kovac J, Leitch E M, Pryke C, et al. 2002 *Nature* **420** 772; Scott P F, Carreira P, Cleary K, et al. 2003 *Mon. Not. R. Aston. Soc.* **341** 1076; Spergel D N, Bean R, Dorè et al. 2007 *Astrophys. J.* **170** 377 *Preprint* astro-ph/0603449
- [3] Colless M M, Dalton G B, Maddox S J, et al. 2001 *Mon. Not. R. Aston. Soc.* **329** 1039; Colless M M, Peterson B A, Jackson C, et al. 2003 *Preprint* astro-ph/0306581; Loveday J (the SDSS collaboration) 2002 *Contemporary Phys.* **43** 437; Tegmark M, Blanton M, Strauss M et al. 2004 *Astrophys. J.* **606** 702–740; Adelman-McCarthy J K, Agueros M A, Allam S S, et al. 2006 *Astrophys. J. Suppl.* **162** 38–48
- [4] Caldwell R R, Dave R and Steinhardt P J 1998 *Phys. Rev. Lett.* **80** 1582; Wetterich C 1988 *Nucl. Phys.* **B302** 668
- [5] Brax P and Martin J 1999 *Phys. Lett.* **B468** 40; Brax P and Martin J 2000 *Phys. Rev.* **D61** 103502; Brax P, Martin J and Riazuelo A 2000 *Phys. Rev.* **D62** 103505
- [6] Carroll S M, Duvvuri V, Trodden M, et al. 2004 *Phys. Rev.* **D70** 043528; Nojiri S and Odintsov S D 2003 *Phys. Rev.* **D68** 123512
- [7] Zlatev I, Wang L and Steinhardt P J 1999 *Phys. Rev. Lett.* **82** 896–899; Steinhardt P J, Wang L and Zlatev I 1999 *Phys. Rev.* **D59** 123504
- [8] Schimd C et al *A&A* **463** (2007) 405 Colombo L P L and Gervasi M *JCAP* **10** (2006) 001
- [9] Ellis J., Kalara S., Olive K.A. & Wetterich C., 1989, *Phys. Lett.* **B228**, 264; Wetterich C., 1995, *A&A* **301**, 321; Amendola L., 2000, *Phys.Rev.* **D62**, 043511; Gasperini M., Piazza F.& Veneziano G., 2002, *Phys.Rev.* **D65**, 023508; Comelli, D. Pietroni M. amd Riotto, *Phys. Lett. B* **571** (2003) 115; Chimento L.P., Jakubi A.S., Pavon D. & Zimdahl W.,2003, *Phys.Rev* **D67**, 083513 Guo Z K, Ohta N and Tsujikawa S 2007 *Phys. Rev. D* **76** 023508; Abdalla E, Abramo L R W, Sodre L J and Wang B *Preprint* arXiv:0710.1198 [astro-ph]; Manera M and Mota D F 2006 *Mon. Not. R. Aston. Soc.* **371** 1373
- [10] J. Khoury and A. Weltman , *Phys.Rev.Lett.* **93** (2004) 17110; S.S. Gubser and J.Khoury, *Phys.Rev.D* **70** (2004) 104001; P. Brax et al., *Phys.Rev.D* **70** (2004) 123518
- [11] Majerotto E, Sapone D and Amendola L (200) astro-ph/0410543 Amendola L, Campos G.C. and Rosenfeld R (2006) astro-ph/0610806
- [12] Wei H and Zhang S N 2006 *Phys. Lett.* **B644** 7 Wei H and Zhang S N 2007 *Phys. Lett.* **B654** 139 *Preprint* astro-ph/0704.3330
- [13] Mainini R, Colombo L P L and Bonometto S A *Astrophys. J.* **632** (2005) 691

- [14] Di Porto C and Amendola L (2007) astro-ph/0707.2686
- [15] M. Doran, J. Jaeckel, Phys.Rev. D **66** (2002) 043519; Amendola L, Quartin M, Tsujikawa S, and Waga I, Phys.Rev. D **74** (2006) 023525
- [16] Amendola L Phys.Rev. D **62** (2000) 043511; Amendola L Phys.Rev. D **69** (2004) 103524
- [17] Huey G and Wandelt B D Phys.Rev. D **74** (2006) 023519; Das S, Corasaniti P S and Khoury J, Phys.Rev. D **73** (2006) 083509
- [18] Amendola L and Quercellini C Phys.Rev. D **68** (2003) 023514 Olivares G, Atrio-Barandela F and Pavon D (2007) astro-ph/0706.3860
- [19] Das S, Corasaniti P S and Khoury J Phys.Rev. D **73** (2006) 083509
- [20] Mainini R and Bonometto S A JCAP (2007) astro-ph/0703303
- [21] Mainini R Phys.Rev.D **72** (2005) 083514
- [22] Amendola L, Kunz M and Sapone D (2007) astro-ph/0704.2421
- [23] Bartelmann M and Schneider P 2001 Phys.Rept. **340** 291
- [24] Refregier A *Ann. Rev. Astron. Astrophys.* 2003 **41** 645
- [25] Van Waerbeke L and Mellier Y *Preprint* astro-ph/0305089
- [26] Schneider P *Preprint* astro-ph/0509252
- [27] Amara A and Refregier A *Preprint* astro-ph/0610127
- [28] Hu W 1999 *Astrophys. J.* **522** L21
- [29] Huterer D 2002 *Phys. Rev. D* **65** 063001
- [30] Hu W and Jain B 2004 *Phys. Rev. D* **70** 043009
- [31] Ma Z M, Hu W and Huterer D 2005 *Astrophys. J.* **636** 21
- [32] Kaiser N 1998 *Astrophys. J.* **498** 26
- [33] Cooray A and Hu W 2001 *Astrophys. J.* **554** 56
- [34] Takada M and Jain B 2004 *Mon. Not. R. Aston. Soc.* **348** 897
- [35] Sivia D S 1996 *Data analysis: A Bayesian Tutorial* (Oxford: Oxford University Press)
- [36] Fisher R A 1935 *J. Roy. Statist. Soc.* **98** 39
- [37] Tegmark M, Taylor A and Heavens A 1997 *Astrophys. J.* **480** 22
- [38] Oh S P, Spergel D N and Hinshaw G 1999 *Astrophys. J.* **510** 551
- [39] Matsubara T and Szalay A S *Preprint* astro-ph/0203358.
- [40] Refregier A et al. *Preprint* astro-ph/0610062
- [41] Rudd D H, Zentner A R and Kravtsov A V *Preprint* astro-ph/0703741. Zentner A R, Rudd D H and Hu W 2008 *Phys. Rev. D* **77** 043507
- [42] <http://www.camb.info/>
- [43] Smith R E, et al. 2003 *Mon. Not. R. Aston. Soc.* **341** 1311
- [44] Mainini R 2005 *Phys. Rev. D* **72** 083514
- [45] Maccio A V Quercellini C Mainini R Amendola L and Bonometto S A 2004 *Phys. Rev. D* **69** 123516
- [46] Ratra B and Peebles P J E 1998 *Phys. Rev. D* **37** 3406
- [47] Ma Z M *Preprint* arXiv:astro-ph/0610213.
- [48] Eisenstein D J Hu W and Tegmark M 1999 *Astrophys. J.* **518** 2